Review

Advances of Biowaste-Derived Porous Carbon and Carbon–Manganese Dioxide Composite in Supercapacitors: A Review

Akzhibek Zekenova [1,2]**, Meruyert Nazhipkyzy** [1,3,4,]*****, Wanlu Li** [5]**, Akmaral Kalybayeva** [6]**, Guldarikha Zhumanova** [7] **and Olga Zubova** [7]

[1] Department of Chemical Physics and Material Science, Al-Farabi Kazakh National University, Almaty 050040, Kazakhstan
[2] Engineering Academy, RUDN University, 117198 Moscow, Russia
[3] Institute of Combustion Problems, Almaty 050012, Kazakhstan
[4] Department of Materials Science, Nanotechnology and Engineering Physics, Satbayev University, Almaty 050013, Kazakhstan
[5] Department of Chemistry, Saint Peter's University, Jersey City, NJ 07306, USA
[6] Engineering-Technological Institute, Korkyt Ata Kyzylorda University, Kyzylorda 120000, Kazakhstan
[7] Department of Geography and Environmental Sciences, Al-Farabi Kazakh National University, Almaty 050038, Kazakhstan
***** Correspondence: meruert82@mail.ru; Tel.: +7-775-900-42-48

Abstract: One of the global problems is environmental pollution by different biowaste. To solve the problem, biowaste must be recycled. Waste-free technology is also a way of saving exhaustible raw materials. Research on electrochemical energy sources is currently the most dynamically developing area of off-grid energy. Electrochemical capacitors can operate for a long time without changing performance, they have smaller dimensions, high mechanical strength, and a wide operating temperature range. These properties are effective energy-saving devices. Therefore, supercapacitors are widely used in various industries. This review discussed the methods of obtaining and the characteristics of biowaste-derived activated carbon and carbon–manganese oxide (AC-MnO_2)-based supercapacitor electrodes.

Keywords: supercapacitor electrodes; biowaste; activated carbon; MnO_2; composite

1. Introduction

Currently, there is a growing demand for various energy storage devices, which drives research to develop energy storage systems with a high efficiency at lower costs [1,2]. Compared to other energy storage devices, supercapacitors can possess a fast charge/discharge feature, long cycling life, excellent reversibility, high power density, and wide temperature range operation. Due to these characteristics, supercapacitors are widely used in consumer electronics that require a burst of power density. It can also be utilized as power supplies for portable devices such as notebooks, smartphones, and computers [2,3].

Supercapacitors, known as electrochemical capacitors (ECs) or ultracapacitors, are a new electrochemical energy storage system that stores energy by charge accumulation [4]. Supercapacitors are classified into electric double-layer capacitors (EDLC) that are based on non-faradic processes—pseudocapacitors (PC), that are based on faradic processes, and hybrid capacitors (HC), which combines two types of the above charge storage mechanism. Supercapacitors can also be categorized into two types according to the arrangement of electrodes: symmetric capacitors have both anodes and cathodes identical to each other, and asymmetric capacitors are made of two different materials [5].

The choice of raw materials affects the supercapacitor type and the desired electrochemical characteristics.

Figure 1 below classifies the type of supercapacitor according to the electrode materials. Recently, scientists have paid more attention to obtaining electrode materials from non-conventional raw materials. The use of non-conventional raw materials can simultaneously reduce the cost and environmental pollution.
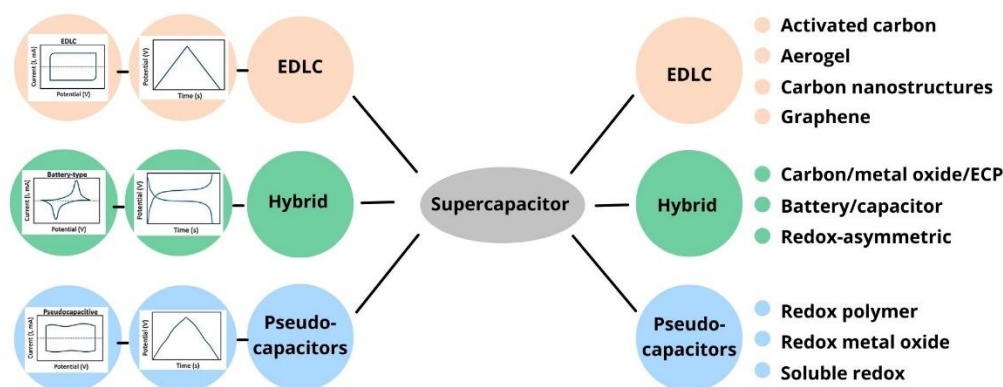

Figure 1. Different classes and subclasses of supercapacitors based on the electrode materials.

As shown in Figure 1, carbon materials, metal oxides, conductive polymers, and various composite materials are used as electrode materials. Different types of carbon materials (such as graphite, graphene, and carbon nanotube) have been applied as a supercapacitor electrode material due to its extraordinary properties, such as high electrochemical stability and high electrical conductivity [6,7]. However, these electrode materials have their disadvantages. For instance, graphene sheets have a high specific surface area, effective charge storage transport properties, and a wide potential window. They quickly form irreversible agglomerates and restack to their graphite structure, and the determination of intrinsic capacitance becomes very difficult [8]. Despite the superior mechanical and electrical properties of carbon nanotubes (CNTs), one of the main challenges in applications is their difficulty forming homogeneous dispersion, which weakens the electrode's mechanical, electrical, and chemical properties. Applying these materials is hindered by the prevailing time-consuming and energy-wasting procedures. Because of this, it is preferable to use biowaste-derived carbon materials since they are easily accessible, renewable, and sustainable [7]. Among the above carbon materials, activated carbon (AC) is a popular commercial supercapacitor electrode material due to its low cost, high specific surface area, high electrochemical stability, and high electrical conductivity [6].

The specific capacitance and energy density of EDLCs cannot compete with pseudocapacitors, owing to their inherent electrostatic surface charging mechanism. Therefore, an effective way to prepare high-performance composite electrode materials is combining various functional carbon materials and typical metal oxides or conductive polymers [9]. To date, transition metal oxides have displayed pseudocapacitive behavior with high specific capacitance and multiple oxidation states that make them advantageous for supercapacitor applications [10]. Commonly used transition metal oxides are Fe_2O_3, MnO_2, ZnO, NiCo layered double hydroxides, CoAl layered double hydroxides, and Co_3O_4; in addition, their composites have been widely studied [11]. Manganese dioxide (MnO_2) is an excellent pseudocapacitive electrode material among other advanced transition metal ox-

ides due to the electrochemical abilities, varied range of potentials, natural wide occurrence, environmentally benign property, and theoretical capacitance value (1380 F/g) [12,13]. MnO_x can have a higher capacitance than carbon materials because it possesses faradaic or pseudocapacitance, resulting from fast redox reactions occurring at the interface between metal oxides and electrolytes, in addition to the double-layer capacitance. However, the low electrical conductivity, strong agglomeration, and poor cycle life of metal oxides limit their use in high-capacity storage devices. The use of hybrid active materials consisting of a metal oxide and a carbon host is a promising approach to solve these problems [14]. Therefore, this article will consider activated carbon synthesized from biowaste and carbon–manganese oxide composite materials.

This article reviewed the types, the obtaining methods of biowaste-derived activated carbon and its composite based on MnO_2, considered the influence of different crystal structures of MnO_2 on the structure of activated carbon which affects the supercapacitor performance, and briefly described the characteristics of commercial supercapacitors. This article is a brief review about biowaste-derived activated carbon and its composite based on MnO_2, and we hope to help students and scientists who are well versed in this topic.

2. Raw Materials

The raw material is essential for obtaining high-quality electrodes. To synthesize activated carbon, the carbon content must be high in the raw material because it will affect the yield of the product. It is also crucial to choose raw materials with low impurities or easily removable impurities. The raw material composition should not contain any toxic compounds for safety reasons.

Two types of raw materials are used to obtain activated carbon: non-conventional and conventional activated carbon. Traditional raw materials include wood, peat, bituminous coal, lignite, petroleum coke, and pitch [15–22]. Table 1 lists characteristics of some carbon-based supercapacitor electrodes from fossil fuels, such as, petroleum, coke, coal, and pitch. Despite the high quality of the obtained carbon, the non-conventional raw materials have some disadvantages, namely, the decreasing availability of fossil fuels, the growing global energy demand, and increased awareness of the environmental impacts of fossil fuel combustion [22]. Therefore, scientists have recently obtained electrode materials from renewable raw materials, mainly waste [23].

To not recycle household waste pollutes the environment and is still an actual problem. In addition to industrial pollution, the environment is also polluted by wood products [24]. To tackle this issue and save non-renewable resources, it is essential to use different types of waste.

Table 1. Fossil fuels obtained activated carbons for supercapacitor electrodes.

Raw Material	S_{BET} (m²/g)	Current Density (A/g)	Specific Capacitance (F/g)	Types of Test Cells	Reference
Petroleum coke	2964	0.05	220	Two-electrode cell with symmetrical electrodes.	[25]
Coal	1032	0.5	108	Three-electrode cell with Hg/HgO as the reference electrode, AC as the working	[26]
Pitch	3145	0.05	272	electrode and platinum plate as the counter electrode. Two-electrode cell with symmetrical electrodes.	[27]

Non-Conventional Biowaste Raw Materials

Recently, renewable biowaste-derived activated carbons have attracted significant attention due to their interesting characteristics of naturally porous or hierarchical structured and heteroatom doping [28]. This biowaste-derived activated carbon has reduced electrochemical properties compared to carbon fibers, commercial activated carbon, CNTs, etc. However, their major advantage is low cost, ease of production, environmental friendliness, and the presence of their inherent functional groups and heteroatoms, which makes them a suitable substitute for carbonaceous materials derived from fossil fuels. Biowaste-derived activated carbon has been identified as a suitable electrode for energy storage devices due to its required pore size, large specific surface area, low equivalent series resistance, and high stability [29].

Non-conventional raw materials are very diverse, and most of them could be easily found in daily lives, such as food waste (coconut shell [30], pecan nutshell waste [31], ginkgo shells [32], onion peel [33], pomelo peel [34], garlic peel [35], orange peel [36], etc.), animal waste (crab shell [37], pork bone [38], blackfish bone [38], eel bone [38], fish bladder [39], etc.), plant waste (Couroupita guianansis [40], Elm flower [41], kapok flower [42], hemp stem [43], pine cones [4], banana leaves [44], etc.). Figure 2 illustrates the types of biowaste-derived activated carbon. Notably, the raw material types increase yearly due to the demand for activated carbon-based supercapacitors.

Currently, scientists also synthesize activated carbon for the supercapacitor not only from biowaste, for instance, Coca-Cola waste [45], tires [46], tobacco waste [47], plastic bags, and other industrial wastes [48]. Due to the pandemic, the amount of used masks has increased, and scientists in China synthesize carbon from the covers for the supercapacitor electrodes [49].
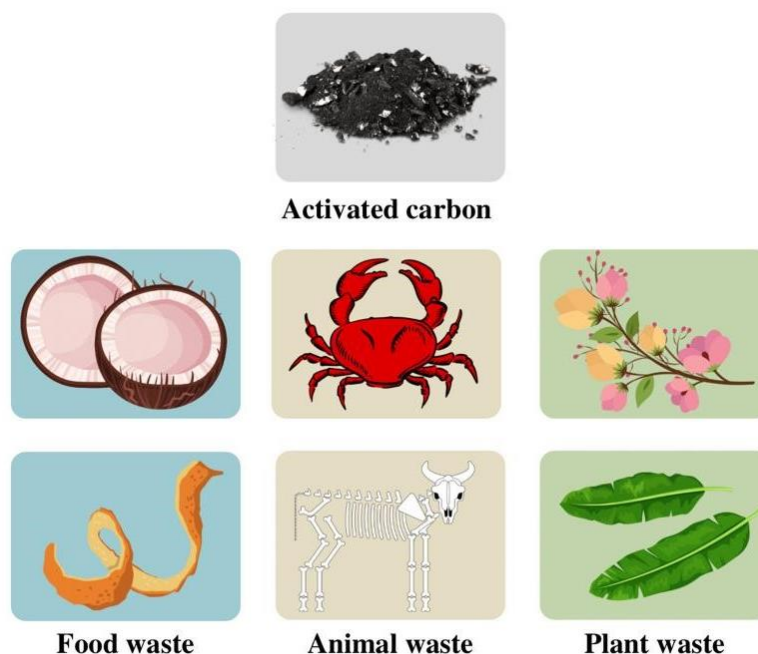
Figure 2. The types of biowaste-derived activated carbon.

The properties of biowaste determine the properties of the derived activated carbon, and consequently, the supercapacitor electrode characteristics. Therefore, choosing the proper biowaste organ/tissues is also essential. Biowaste generally consists of organic substances (saccharides, vitamins, fatty acids) and other elements (H, O, N and S). Besides C, O, H, S, and N, some minerals, such as Ca, K, Mg, Na, and Si, may also be contained in

the biowaste. The thermal pyrolysis or carbonization process decomposes large quantities of organic matter into H_2O and CO_2 and forms pores. Other elements can also be removed by thermal conversion to some extent. Therefore, activation is used to obtain porous carbon with a high carbon concentration [50]. The composition may also vary according to the raw material location (country, etc.). For instance, biowaste from saline–alkali land is rich in mineral elements such as, Ca, K, Mg, Na, and Si [6, 50].

The raw material is usually pre-treated before carbonation. The biowaste pre-treatment depends on the type of raw material. Currently, there are several types of raw material pretreatment. It includes physical pretreatment (coarse size reduction, chipping, shredding, grinding, milling), biological pretreatment (the action of fungi capable of producing enzymes that can degrade lignin, hemicellulose, and polyphenols), chemical pretreatment (with acids, alkali, organic solvents, and ionic liquids), and physicochemical pretreatment (use of conditions and compounds that affect the physical and chemical properties of biowaste) [51]. In order to make homogeneous and reproducible carbons, the precursors need to be pre-treated through careful grinding and purification [23].

Table 2 lists characteristics of some carbon-based supercapacitor electrodes from biowaste.

Table 2. Biowaste-derived activated carbon and AC-based electrodes for supercapacitor.

Raw Material	S_{BET} (m^2/g)	Current Density (A/g)	Specific Capacitance (F/g)	Types of Test Cells	Reference
Plant waste					
Sugarcane bagasse	725	0.2	265	Three-electrode cell (working (AC), reference (saturated calomel electrode), a counter (Pt wire).	[52]
Elm flower	2048.6	20	216	Two-electrode cell with symmetrical electrodes.	[41]
Kapok flower	1904.1	1	286.8	Three-electrode cell (counter (Pt wire), reference electrode (Ag/AgCl), working (AC) cell.	[42]
Sakura petals	1433.8	0.2	265.8	Three-electrode working (AC), counter (Pt sheet), reference (a saturated calomel electrode).	[53]
Lignin	1425	10 mV/s	140.9	Three-electrode cell (working (AC), counter (Pt), and references (Ag/AgCl)).	[54]
Food waste					
Garlic peel	3325.2	1	424.42	Two-electrode cell with symmetrical electrodes.	[35]
Onion peel	3150	0.5	169	Three-electrode cell (working (AC), counter (glassy carbon), and references (Ag/AgCl)).	[33]
Pomelo peel	1582	0.5	180	Three-electrode cell (reference (Hg/HgO), a counter (graphite sheet), working (porous carbon)).	[34]
Orange peel	1391	0.5	407	Three-electrode cell (working (porous carbon), counter (Pt strip), and reference (saturated calomel electrode).	[36]
Animal waste					
Crab shell	3442	0.2	280.6	Two-electrode cell with symmetrical electrodes.	[37]

Pork bone	1260	0.5	263	Three-electrode cell (working (AC), counter (Pt foil), reference (saturated calomel electrode)).	[38]
Blackfish bone	1202	0.5	302	Three-electrode cell (working (AC), counter (Pt foil), reference (saturated calomel electrode)).	[38]
Eel bone	1163	0.5	264	Three-electrode cell (working (AC), counter (Pt foil), reference (saturated calomel electrode)).	[38]

By comparing Tables 1 and 2, we can observe that biowaste materials are excellent for a supercapacitor, and by using biowaste materials, we can even obtain a supercapacitor with a comparatively higher capacity than with fossil fuels that have obtained activated carbon [25–27,55]. Depending on the method of obtaining them (such as temperature, activation time, activation type, activating agents etc.), different types of biocarbon behave differently as supercapacitors.

3. Electrode Materials

3.1. Biowaste-Derived Activated Carbon

Activated carbon is the most used material for EDLC electrodes with moderate cost that have a complex porous structure comprising micropores (smaller than 2 nm), mesopores (in the range of 2–50 nm), and macropores larger than 50 nm, leading to the high specific surface area. AC shows physicochemical properties based on raw materials and activation methods, which strongly influence its surface area, porous structure, and pore size distribution [56]. Generally, porous carbon is produced by a two-step process: carbonization followed by activation. In the first step, carbon precursors are heated to temperatures between 400 °C and 1000 °C in an inert gas atmosphere. Low porosity carbons can be obtained after the carbonization process. Further, an activation process is used to increase the porosity of carbon materials. Usually, three methods can be used in the activation process: physical activation, chemical activation, and physicochemical activation. Oxidizing gases such as CO_2, O_2, air, or H_2O are used in physical activation at high temperatures (up to 900 °C) by reacting with the carbon atom to obtain porous carbon. The physical activation process can be considered partial gasification of the carbon precursor matrix [57]. The physicochemical activation process involves the chemical impregnation of carbon precursors with activating agents, followed by a physical activation step under an oxidizing gas atmosphere. The process is complex and has excessive energy consumption. Of these three methods, chemical activation is considered the most perspective method for producing ACs with excellent performance [58].

3.1.1. Physical Activation

Physical activation consists of carbonization at a low temperature in an inert atmosphere and activation at a high temperature using an activating reagent [59]. The carbonization process removes non-carbon elements such as hydrogen and oxygen, and leads to a carbon skeleton (char) with a rudimentary pore structure. The carbonization temperature, heating rate, and soaking time are the main experimental parameters determining the yield of the process. The incipient porosity of the carbonized material becomes blocked by the tar produced in the thermal process. Therefore, the activation process is necessary to remove the tar blocking the pores and improve the specific surface area or pore volume. This is carried out by a reaction with oxidizing reactants (carbon dioxide, steam, and mixtures of them are the most frequently employed) at temperatures ranging from 800 °C to 1000 °C [58,60]. The process involves the interaction of steam, gas, or a mixture of steam and gas (activating agent) with carbonized carbon [61]. The choice of activating agent also

depends on the precursor material because different materials require a different activating agent to obtain a high surface area. The development of a porous structure is the primary purpose of the activating agent, and this is usually achieved by a controlled combustion of carbon and the elimination of volatile matters. The degree of carbon burnout is strongly dependent on the temperature and duration of activation time. Other experimental parameters such as the gas flow rate and the type of furnace ultimately determine the quality of the activated carbon [59]. It has been experimentally verified that physical activation can be carried out in one step by combining carbonization and activation. The two-step process (carbonization and activation) can be simplified by carbonizing the raw material under a stream of N_2 and replacing the N_2 with an oxidizing gas (steam/CO_2) after carbonization; this is conducted without cooling the product, and only reaching the desired activation temperature. This process is cheaper and faster than the two-step physical activation [61]. Table 3 presents the characteristics of biowaste-derived activated carbon obtained by physical activation.

Some factors are affecting the rate of gasification carbon with oxidizing gases. They are the reaction temperature, the partial pressure of the reacting gas, hydrogen and carbon monoxide that inhibit gasification reactions, inorganic compounds in carbon acting as positive oxidation catalysts, and the structure of the carbon source [62].

Table 3. Physical activation of various biowaste. Adapted with permission from Ref. [61]. 2019, Ayinla, R.T. and etc.

Raw Mterial	Agent	Temperature (°C)	BET (m²/g)	V_{Micro} (m³/g)	Reference
Barley straw	CO_2	800	789	0.3268	[63]
Palm shell	CO_2	850	1653	0.8900	[64]
Coconut shell	steam	900	1194	0.4460	[65]
Artrocarpus waste	steam	750	917	0.4800	[66]
Acorn shell	CO_2/steam	600	1799	0.9270	[67]

Based on Table 3, we can see that by using a combination of activators [67], the material achieves the largest surface area (1799 m²/g) and micropore volume (0.9270 cm³/g), while the smallest micropore volume (0.3268 cm³/g) and surface area (789 m²/g) is achieved by the activation with CO_2 [63], which is not preferable for the electrochemical performance of the supercapacitor. Based on this table, we suppose that the activator mixture is more suitable for creating an electrode because a large specific surface area and micropore volume are important for the supercapacitor.

Physical activation is an inexpensive method to produce activated carbon. It is considered an environmentally friendly approach because it does not contain chemical agents. However, the main disadvantages of the process are the long activation time and high energy consumption. The activated carbons also show low adsorption capacity [68].

3.1.2. Chemical Activation

Chemical activation is the most used and promising method due to the low heating temperature, short processing time, high carbon yield, well-controlled porosity, and high specific surface area of AC [58]. Chemical activation is usually used for cellulose materials, such as biomass resources. In the chemical activation to prepare activated carbon, the raw material was activated with activating agents at high temperatures [68].

The raw material is crushed and milled, then mixed with a concentrated solution of a dehydrating agent. The mixture is dried and heat-treated under an inert atmosphere at temperatures between 400 °C and 700 °C [60]. The resulting activated carbons need to be washed with acid and/or water to lower the ash content further and remove the activated

carbon's residual chemicals [69]. Then, the product is separated from the slurry, dried, and conditioned according to its application [60].

According to the acid-basic theory and activation mechanism, activating agents can be classified into four types: alkaline (KOH [70], NaOH [71], K_2CO_3 [72], K_2SiO_3 [73]), acidic (H_3PO_4 [74], H_3PO_3 [75], H_2SO_4 [76], $C_3H_9O_4P$ [77]), neutral ($ZnCl_2$ [78], KCl [79]), and self-activating agents [58]. It is important to note that there are only three activating agents ($K_3C_6H_5O_7$ [80], $C_6H_{11}KO_7$ [81]) based on the activation mechanism. The activating agents' role is to degrade the cellulosic material by thermal treatment. The dehydrating agents inhibit the formation of tar and other by-products [60]. The activation temperature also depends on the type of activating agent. An excessively high activation temperature can reduce carbon yield and specific surface area, and an excessively low activation temperature may result in a poor porous structure. The optimal activation temperature using acid activation agents is generally in the range of 400–500 °C. The optimal activation temperature using alkaline and self-activating agents is generally in the range of 750–850 °C [58]. Table 4 presents the characteristics of biowaste-derived activated carbon obtained by chemical activation.

The inert gases protect the carbon precursor's burnout and transfer the resulting pyrolysis gases outside the furnace [58]. The porosity of activated carbon is also affected by the activation atmosphere; the use of an oxidant atmosphere instead of an inert atmosphere produces activated carbon with a larger surface area and an increased mesopore volume due to the expansion of pores during activation [82].

The conventional method of chemical activation has the following disadvantages: severe corrosion of the reactor, small pore size, destruction of the pore structure, and environmental impact. Scientists develop new methods to solve these problems. According to the different activation mechanisms, these new methods are molten salt, degradable salt, and the oxidizing salt method. Molten salt etching techniques use corrosive molten chemical agents ($CuCl_2$, $NiCl_2$, NaCl, KCl, $FeCl_3$) to react with carbon to create porous structures at high temperatures. The different salts decompose, and thus, the decomposition gases can etch the carbon to form pores. Salts such as $Zn(NO_3)_2$, $NaNO_3$, $MgCO_3$, K_3PO_4, NaH_2PO_4 are used in the decomposition etching method. The oxidative salt etching method can also achieve the pore engineering of carbon materials. Oxidative activators such as HNO_3, $KMnO_4$, KNO_3, and $Mn(NO_3)_2$ have been used to obtain porous carbon by oxidation of carbon at room temperature or high annealing temperatures [83].

Table 4. Chemical activation of various biowaste.

Raw Material	Agent	Activation Temperature (°C)	S_{BET} (m²/g)	V_{Micro} (cm³/g)	Reference
Alkaline					
Apricot shell	NaOH	700	2335.00	0.797	[84]
Rice husk	NaOH	800	2682.00	1.011	[85]
Rice straw	KOH	800	1917.00	0.730	[86]
Acidic					
Walnut shells	H_3PO_4	400	2095.00	0.520	[87]
Sunflower oil cake	H_2SO_4	600	240.02	0.111	[88]
Neutral					
Date pits	$FeCl_3$	700	780.00	0.468	[89]
Pine-fruit residue	$ZnCl_2$	500	774.20	0.305	[90]

Based on Table 4, the most excellent activators are alkaline [84–86] because the carbons result in a large specific surface area and the volume of micropores. We suppose that the least suitable activators are the neutral agents [89, 90]; activation with acid [87, 88] is also great for creating electrode material but requires the right obtaining approach. By comparing Tables 3 and 4, it can be concluded that chemical activation is preferable to develop a comparatively high-quality activated carbon from biowaste for the supercapacitor.

Based on Tables 3 and 4, it can be concluded that the activation method affects the porosity and specific surface area; according to the authors, chemical activation and activator mixture are better suited to obtain AC, since a large specific surface area and micropore volume are reached by activation.

It should be mentioned that the surface functional groups of activated carbon can also affect the performance of the supercapacitor, which may depend on the method of obtaining AC, the electrolyte used, etc. For example, scientists in [91] work modified the AC by $(NH_4)_2S_2O_8$ oxidation; their results indicate that the oxygen functional groups, especially carboxyl and carbonyl groups, improved the wettability of the pore surfaces, increased the electrolyte diffusion rate into the electrode, and increased the specific capacitance by an additional pseudo-capacitance in a 6 mol/L KOH aqueous electrolyte; excess oxygen content blocked the pores, leading to poor electrochemical performance, but annealing at 300 °C in an inert atmosphere increased the specific capacitance and improved the rate performance in a 6 mol/L KOH aqueous electrolyte. However, organic electrolyte oxygen functional groups reduced the specific capacitance. In [92], scientists obtained the activated carbon from argan seed shells by KOH activation. AC induced oxygen and nitrogen groups on the surface and the experimental findings show that nitrogen-enriched activated carbons exhibited the highest capacitance and retention of 355 F/g at 125 mA/g and 93% at 1 A/g, respectively, compared to oxygen-doped activated carbons. Results show that surface carboxyl functionalities in oxygen-enriched activated carbons prevent electrolyte diffusion into the porous network, while the existence of nitrogen groups can produce micro-mesoporosity and excellent pseudo capacitance properties [93]. Functional groups are claimed as the most responsible for performance degradation and ageing of activated carbon in organic electrolytes. These functionalities (mainly carboxylic, lactone, or phenolic groups) are thought to be harmful in organic electrolytes but beneficial in aqueous-based electrolytes, where they can provide an extra capacitance through a pseudocapacitive mechanism; however, scientists proved that the functionalities on the surface of activated carbon contribute to the capacitance through pseudo-redox reactions in the organic electrolytes and can also be beneficial for inhibiting the potential shift of AC [94]. Based on the above, we can conclude that activation methods and types of electrolyte can affect the performance and efficiency of the supercapacitor, since one sample can show different characteristics in organic- and aqueous-based electrolytes due to the functional groups.

3.2. AC-MnO$_2$ Composites

There are several crystallographic structures of MnO_2, such as α, β, γ, ε, and δ forms, depending on the way a MnO_6 octahedral interlinks with another. The polymorphism of MnO_2 can be controlled by the synthesis conditions. Since capacitive properties are due to the intercalation/deintercalation of protons or cations in MnO_2, only specific crystallographic structures can be helpful for capacitance studies. Devarai et al. reported that the particular capacitance measured for MnO_2 decreases in the following order $\alpha \approx \delta > \gamma > \lambda > \beta$ [95].

Research has shown that the chain or tunnel structure of MnO_2 with a large two-dimensional tunnel structure facilitates electron transfer, providing a relatively high capacitance value [9]. The large surface area of δ-MnO_2 with a layered or sheet-like structure is more favorable for cation intercalation/deintercalation than an amorphous structure.

The three-dimensional hinge structure of λ-MnO_2 can provide more active sites for improved electrochemical properties. However, MnO_2 has disadvantages such as low conductivity, poor ion diffusion constant, and poor structural stability. Therefore, a high reversible capacitance, structural stability, and fast cation diffusion at high charge/discharge rates should be improved, and deterioration volume expansion can be avoided [96, 97].

The combination of coal and manganese oxide shows a synergistic effect by combining the double layer capacitance and the redox capacitance. The high specific surface area of carbon substrates provides a large number of anchoring sites for the loading of MnO_2 and increases the contact interfaces between MnO_2 and the electrolyte. It should be noted the porous carbon with well-ordered pore channels provides a fast electrolyte transfer throughout the composite electrode, facilitating a smooth access of electrolyte ions to the active MnO_2 during the charge/discharge process. An important factor is the loading content of MnO_2 [98].

After modification by δ-MnO_2, many aggregated manganese dioxide blocks on the surface of activated carbon were observed, and surface area, total pore volume, and average pore size were decreased (Figure 3a) [99].
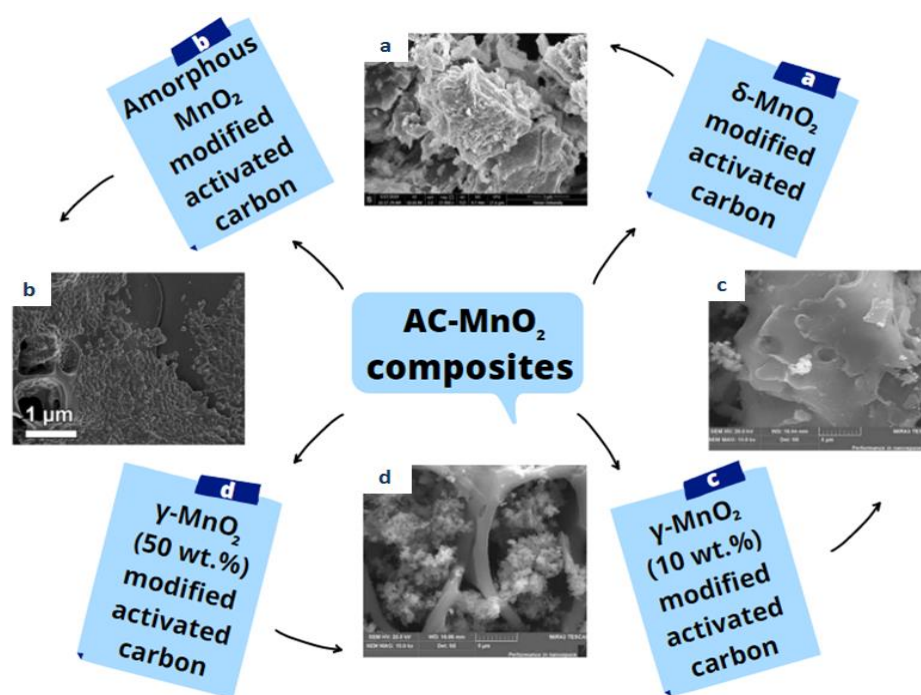

Figure 3. Scheme of AC/MnO_2-based composite types: (**a**) δ-MnO_2-modified activated carbon. This figure is reprinted from [99], with permission from Elsevier B.V., 2022; (**b**) amorphous MnO_2-modified activated carbon. This figure is reprinted from [95], with permission from Elsevier, 2022; (**c**) γ-MnO_2 (10 wt.%)-modified activated carbon. This figure is reprinted from [100], with permission from corresponding author Prof. Xiaolan Song; (**d**) γ-MnO_2 (50 wt.%)-modified activated carbon. This figure is reprinted from [101], with permission from the corresponding author, Prof. Xiaolan Song. This figure was created by using the Canva application.

The surface of non-modified activated carbon was rough and irregular, and large numbers of pores and carbonaceous blocks were observed. The amorphous nanostructures of MnO_2 were evenly spread over the activated carbon. Nanostructures did not exhibit any particular shape, and their sizes were very different. The bigger particles were completely interspersed with smaller particles (Figure 3b) [100]. As shown in Figure 3, the composite structure was also dependent on the manganese oxide concentration/content. The composite structure was dependent of MnO_2 concentrations/contents. Figure 3c shows the composite with low MnO_2 content; here, there was only a small amount of γ-MnO_2 deposited on the surface of rice husk-derived activated carbon with well-developed

porosity. With the increment of γ-MnO₂ content, it began to deposit in pores and when the γ-MnO₂ content was too high (such as 50 wt.%), it would block pores, thus, potentially reducing composite quality (Figure 3d) [101].

3.3. Methods of Obtaining AC-MnO₂ Composites

There are different methods to prepare composites, for example: precipitation methods such as chemical co-precipitation [96] (indirect, direct, acid-assisted grafting oxidation, etc.), in situ precipitation, and electrodeposition (anodic [102] or cathodic). Table 5 presents the performance of biowaste-derived AC-MnO₂-based supercapacitor electrodes.

Table 5. Biowaste-derived AC and MnO₂ composite-based electrodes for the supercapacitor.

The Raw Material of AC	Current Density	Specific Capacitance	Types of Test Cells	Reference
Banana peel	10 A/g	70 F/g	Three-electrode cell (counter (Pt wire), reference (a saturated calomel), working (composite)).	[103]
Bamboo	1 A/g	221.45 F/g	Three-electrode cell (counter (Pt plate), reference (a saturated calomel), working (composite).	[104]
Faidherbia albida shell	1 A/g	426.66 F/g	Three-electrode cell (counter (Pt wire), reference (Ag/AgCl), working (composite).	[105]
Rice husk	0.2 A/g	977.4 C/g	Two-electrode cell with symmetrical electrode).	[106]
Rice husk	0.5 A/g	210.3 F/g	Three-electrode cell (counter (Pt plate), reference (saturated calomel), working (composite).	[107]
Wheat bran	1 A/g	258 F/g	Three-electrode cell (counter (Pt foil), reference (Ag/AgCl), working (composite).	[108]
Lignin	10 mV/s	345.3 F/g	Three-electrode cell (working (composite), counter (Pt), and references (Ag/AgCl)).	[54]
Corncob	-	1281.3 mF/cm²	Three-electrode cell (working (composite), counter (Pt plate), and references (Ag/AgCl)).	[109]

In the indirect co-precipitation method, AB was first mixed with the solution of HNO₃ and Mn(NO₃)₂·4H₂O. After the reaction, the mixture was vacuum filtered and washed to remove unreacted Mn(II) cations. The impregnated AB was then mixed with KMnO₄ in deionized water. The nanocomposite was then separated from the mixture, rinsed, and dried [96].

In the acid-assisted grafting oxidation co-precipitation method, AB was first acid-activated by a mixture of pure acid and water and was stirred. After sonicating the suspension, the mixture was heated in an oven. The filtered sample was washed and dried. The AB-MnO₂ nanocomposite was then synthesized following the direct co-precipitation method [96].

Tianfu fabricated MnO₂ and decorated the bamboo-based activated carbon by an in situ preparation method. To prepare a certain amount of AC, MnO₂ was dispersed in an aqueous solution under ultrasonication and heated in an oil bath in an autoclave, then the product was centrifuged, washed, and dried [104].

Yuan prepared the composite by an in situ precipitation method. A certain amount of surface-modified rice husk-derived activated carbon and MnSO₄ were dispersed in propyl alcohol through ultrasonication, then the liquid was heated. Afterwards, KMnO4

dissolved in deionized water and was added to the mixture. The product was obtained by filtration and dried in an oven [107].

From the study of Adorna J. et al. [96], coconut shell-derived activated biochar (AB) was hydrothermally synthesized and then was coupled with manganese dioxide (MnO_2) from different co-precipitation methods to form nanocomposites. For the direct preparation of AB-MnO_2 nanocomposites, AB was combined with the solution of acid and $Mn(Ac)_2 \cdot 4H_2O$; the mixture was stirred under a water bath. After the reaction, $KMnO_4$ was then added dropwise. The sample was vacuum filtered, rinsed, and dried.

In [54], to obtain the composite material, the ratio of lignin and surfactant (Pluronic F-127) was 120 wt.%, and the $Mn(NO_3)_2 \cdot 4H_2O$ content was varied to obtain 5, 10, and 20 wt.% Mn in porous carbon. The material and lignin with a Pluronic of 120% and manganese oxide of 20% were surface oxidized using 15% *v/v* of H_2O_2.

In [103], the banana peel-derived carbon/MnO_2 was synthesized by a hydrothermal method. A 3D porous carbon was immersed into the $KMnO_4$ solution (a certain amount of $KMnO_4$ and urea were dissolved into 60 mL of deionized water), then the mixture was maintained at 120 °C in the autoclave for 12 h. The sample was washed and dried.

In [106], the hydrothermal method was used in order to obtain AC and MnO_2 composite based on rice husk. To obtain a certain amount of $MnO_2 \cdot H_2O$ and $KClO_3$, they were dispersed in deionized water, then AC was added into the solution and was ultrasonically treated. Afterwards, the sample in the autoclave was heated, and the obtained product was washed and dried.
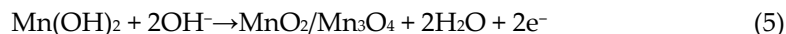
Kong [108] obtained the composite by an in situ hydrothermal method. Wheat bran-derived AC was added into the 0.03 mol L^{-1} $KMnO_4$ solution. After stirred for 1 h, the mixture in the autoclave was heated, then the composite was washed, filtered, and dried.

In [109], the composite was prepared by anodic electrodeposition. It was achieved by using a Pt plate as a counter electrode and Ag/AgCl electrode as a reference electrode. Before electrodeposition, the AC electrode was soaked in the electrolyte containing 0.1 M of $Mn(CH_3COO)_2$ and 0.1 M of Na_2SO_4 for one night. A constant current (1 mA/cm^2) was applied to ensure the growth of MnO_2 nanosheets on the AC membrane. After the as-prepared samples were rinsed gently by the water, they were vacuum dried at 60 °C to obtain the electrodes.

In [102], manganese dioxide (MnO_2) was deposited on the AC electrode by the anodic electrodeposition method using a potentiostat with a three-electrode cell. The pre-treated AC electrode was oxidized in manganese acetate solutions in a typical electrodeposition synthesis.

Cathodic electrodeposition was carried out at negative potentials. The deposition reactions occurring at the cathode surface can be realized via two paths: the first one is based on electrolytes containing Mn^{2+}—the electrochemical processes of this path include water electrolysis, electrochemical reduction of oxygen, deposition of $Mn(OH)_2$, and formation of MnO_2. In the initial stage, a negative potential induces the electrolysis of water at the cathode surface, resulting in the formation of hydrogen gas and hydroxyl ions (Equation (1)); simultaneously, the electrochemical reduction of oxygen contributes to the formation of hydroxyl ions (Equation (2)). The hydroxyl ions increases the pH value in the vicinity of cathode, which then leads to the precipitation of Mn hydroxide ($Mn(OH)_2$) (Equation (3)). The final formation of MnO_2 can be obtained through three routes, as follows: (1) the metastable $Mn(OH)_2$ is readily oxidized to MnO_2 in the presence of oxygen (Equation (4)); (2) $Mn(OH)_2$ can be electrochemically oxidized into MnO_2 or Mn_3O_4 solids (Equation (5)); and (3) thermal annealing of $Mn(OH)_2$ in the air at an elevated temperature results in the conversion of MnO_2 via dehydration and oxidation (Equation (4)).

$$2H_2O + 2e^- \rightarrow H_2 + 2OH^- \tag{1}$$

$$O_2 + 2H_2O + 4e^- \rightarrow 4OH^- \tag{2}$$

$$Mn^{2+} + 2OH^- \rightarrow Mn(OH)_2 \tag{3}$$

$$2Mn(OH)_2 + O_2 \rightarrow MnO_2 + H_2O \tag{4}$$

$$Mn(OH)_2 + 2OH^- \rightarrow MnO_2/Mn_3O_4 + 2H_2O + 2e^- \tag{5}$$

Another cathodic electrodeposition path is based on reducing Mn^{7+} species from $(MnO_4)^-$ ions in the solution on the cathode surface, according to reaction (Equation (6)) [110].

$$(MnO_4)^- + 2H_2O + 3e^- \rightarrow MnO_2 + 4OH^- \tag{6}$$
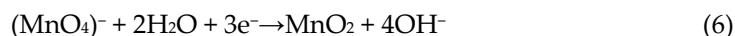
The shape of the nanostructures can be controlled by tuning the deposition parameters. The problem associated with the anodic oxidation and dissolution of inexpensive metal substrates can be avoided by using this technique [98].

Figure 4 shows the preparation scheme of biowaste-derived AC/MnO_2-based composite for supercapacitor electrodes. The biowaste is dried (depending on the type), washed with water or other solutions to remove dirt, and dried to remove moisture. Then, the waste is ground, sieved, and carbonized. The carbon is physically or chemically activated, neutralized, and dried; depending on the method or material, the raw materials may be activated in one step. Depending on the method, a composite is created, washed, and the moisture is removed. To create an electrode, slurry is prepared, and depending on the method of application, supercapacitor electrodes are made.

Figure 4. Scheme of preparation of biowaste-derived AC/MnO_2-based composite for supercapacitor electrodes. This figure was created by using the Canva application.

In [105], electrodes based on Faidherbia albida fruit shell-derived AC and its composite with MnO_2 were obtained. It was found that the hybrid electrode quasitriangular-like shapes had a longer charge-discharge time, which is explained by the smooth redox reaction of electroactive MnO_2 electrolyte solution, which indicates a positive effect of pseudocapacitance material (MnO_2) on specific capacitance. The hybrid composite has a larger symmetrical area under the CV curve for MnO_2/FAFSC. The MnO_2/FAFSC hybrid electrode showed a longer discharge time than the FAFSC electrode. The MnO_2-based electrode could conduct a reversible electrochemical reaction in neutral and alkaline electrolyte solutions. In summary, MnO_2 improves the specific capacitance, which provides a strong synergistic effect and good mechanical reliability to enhance the overall electrochemical performance of the supercapacitor electrode (see Figure 5).
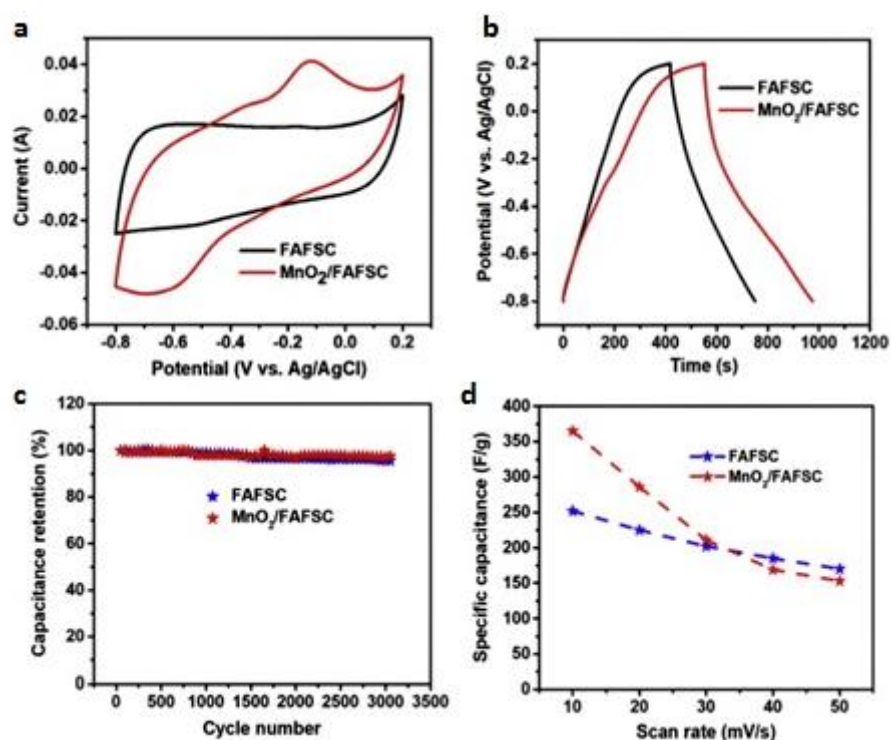
Figure 5. (**a**) FAFSC and MnO₂/FAFCS CV curves at a constant scan rate of 10 mV s⁻¹; (**b**) GCD curves at a constant current density of 6 mA cm⁻² for the FAFSC and MnO₂/FAFSC working electrodes; (**c**) the capacitance retention of the FAFSC and MnO₂/FAFSC composite electrodes at a current density of 40 mA cm⁻² over 3000 cycles; (**d**) the specific capacitance of FAFSC and MnO₂/FAFSC at different scan rates. This figure is reprinted from [105], with permission from Elsevier B.V., 2022.

4. The Performance of Supercapacitors

The performance of supercapacitors is evaluated on the basis of acceptably high energy densities (>10 Wh kg), substantially greater power density, fast charge discharge process (within seconds), excellent cycle stability (more than 100 times of batteries), low self-discharging, safe operation, and low cost [2]. Advanced electrical double-layer capacitors (EDLCs) contain organic electrolytes that operate at 2.7 V, and reach energy densities around 5–8 Wh/kg or 7–10 Wh/L. A commercial corporation offers a 48 V ultra-capacitor module with 1,000,000 duty cycles or a ten-year DC life and 48 V DC working voltage, and the modules are engineered explicitly for hybrid bus and construction equipment to provide cost-effective solutions. Currently, the industry leaders in SC production are Cellergy, Ioxus, Maxwell Technologies, Murata Manufacturing, Nanoramic Laboratories, Nec Tokin, Nippon Chemi-Con, and Panasonic. Supercapacitor devices from these manufacturers have capacitance in the range of 1200–5000 F, low direct current (DC) equivalent series resistance (ESR) values of less than one mΩ, short-circuit current in the range of 600–2400 A, and per cell energy-storage capabilities in the range of 0.6–3 Wh [111].

Nippon Chemi-Con uses activated carbon with a large specific surface area of around 2000 m²/g for the electrodes, and the raw materials of the activated carbon include pitch, resin, and natural plant materials.

After the literature review, we can say that currently activated carbon composite supercapacitors are not yet widely used commercially, while activated carbon supercapacitors, including from biowaste, are in high demand in the commercial sector.

Owing to the two different working mechanisms, EDLCs have a higher cyclic stability or performance. Since an electrode chemical reaction is involved in pseudocapacitors,

irreversible components will accumulate during cycling, leading to deteriorating performance; therefore, the cycling stability of porous carbon will be higher than composites (Table 6) [112].

Table 6. Cycling stability of activated carbon and AC-MnO_2 composite.

Material	Capacitance Retention, %	Reference
Rice husk-derived carbon	98.5 (after 5000 charge–discharge cycles)	[107]
Rice husk-derived carbon/MnO_2	80.2 (after 5000 charge–discharge cycles)	[107]
Bamboo-based activated carbon	99.98 (after 1000 charge–discharge cycles)	[104]
Bamboo-based activated carbon/MnO_2	89.29 (after 1000 charge–discharge cycles)	[104]

SCs have the following advantages: long cycle life, high specific power, quick charge and discharge, and a wide operating temperature range, but the disadvantages may include low energy density, high dielectric absorption, price, and high self-discharge [10, 111].

Due to the advantages of supercapacitors, they are used in the public sector, in automobiles and transportation equipment, in the defense and military industries, in computers and memory backup chips, in medicine and industry, and in power grids for power quality control and battery monitoring [113].

5. Conclusions

To set aside non-renewable raw materials and reduce pollution, different biomass types have been considered as raw materials. The characteristics of electrodes depend on many factors, such as type of biowaste, synthesis techniques, and electrode materials. Therefore, in this review, the biowaste types, the obtaining methods of activated carbon, and the carbon–manganese oxide composite were considered. In addition, the characteristics of activated carbon obtained by chemical and physical activation were also compared, and the comparatively highest result was obtained by chemical activation. In addition, the characteristics of activated carbon obtained with different chemical activating agents were considered and compared, and the most effective activating agents were found to be alkalis and acids. To improve the electrochemical performance of supercapacitor electrodes, the carbon–manganese oxide composite methods were considered, and the characteristics were analyzed. They showed a fast charge–discharge feature, long cycling life, excellent reversibility, high power density, and wide operating temperature ranges.

Author Contributions: Conceptualization, M.N. and W.L.; validation and formal analysis: A.Z.; investigation: A.K.; writing—original draft preparation: M.N. and A.Z.; writing—review and editing, W.L.; visualization: G.Z.; supervision, O.Z.; project administration: M.N. All authors have read and agreed to the published version of the manuscript.

Conflicts of Interest: The authors declare that they have no known competing financial interests or personal relationships that could have appeared to influence the work reported in this paper.

References

1. Sun, K.; Zhang, Z.; Peng, H.; Zhao, G.; Ma, G.; Lei, Z. Hybrid symmetric supercapacitor assembled by renewable corn silks based porous carbon and redox-active electrolytes. *Mater. Chem. Phys.* **2018**, *218*, 229–238. https://doi.org/10.1016/j.matchemphys.2018.07.052.

2. Chang, L.; Hang Hu, Y. Supercapacitors. *Compr. Energy Syst.* **2018**, *2*, 663–695. ISBN 9780128095973.

3. Poonam; Sharma, K.; Arora, A.; Tripathi, S.K. Review of supercapacitors: Materials and devices. *J. Energy Storage* **2019**, *21*, 801–825. https://doi.org/10.1016/j.est.2019.01.010.

4. Manyala, N.; Bello, A.; Barzegar, F.; Khaleed, A.A.; Momodu, D.Y.; Dangbegnon, J.K. Coniferous pine biomass : A novel insight into sustainable carbon materials for supercapacitors electrode. *Mater. Chem. Phys.* **2016**, *182*, 139–147. https://doi.org/10.1016/j.matchemphys.2016.07.015.

5. Barik, R.; Ingole, P.P. ScienceDirect Electrochemistry Challenges and prospects of metal sulfide materials for supercapacitors. *Curr. Opin. Electrochem.* **2020**, *21*, 327–334. https://doi.org/10.1016/j.coelec.2020.03.022.

6. Zhao, Y.; Dong, C.; Sheng, L. Heteroatoms-doped Pillared Porous Carbon Architectures with Ultrafast Electron and Ion Transport Capabilities under High Mass Loadings for High-rate Supercapacitors Heteroatoms-doped Pillared Porous Carbon Architectures with Ultrafast Electron and Ion Tra. *ACS Sustain. Chem. Eng.* **2020**, *8*, 8664–8674. https://doi.org/10.1021/acssuschemeng.0c01661.

7. Sim, G.; De Oliveira, H.P.; Larsson, S.H.; Thyrel, M.; Lima, E.C. A Short Review on the Electrochemical Performance of Hierarchical and Nitrogen-Doped Activated Biocarbon-Based Electrodes for Supercapacitors. *Nanomaterials* **2021**, *11*, 424.

8. Dubey, R.; Guruviah, V. Review of carbon-based electrode materials for supercapacitor energy storage. *Ionics* **2019**, *25*, 1419–1445. https://doi.org/10.1007/s11581-019-02874-0.

9. Wu, D.; Xie, X.; Zhang, Y.; Zhang, D.; Du, W.; Zhang, X.; Wang, B. MnO$_2$/Carbon Composites for Supercapacitor: Synthesis and Electrochemical Performance. *Front. Mater.* **2020**, *7*, 1–16. https://doi.org/10.3389/fmats.2020.00002.

10. Afif, A.; Rahman, S.M.; Tasfiah Azad, A.; Zaini, J.; Islan, M.A.; Azad, A.K. Advanced materials and technologies for hybrid supercapacitors for energy storage—A review. *J. Energy Storage* **2019**, *25*, 100852. https://doi.org/10.1016/j.est.2019.100852.

11. Ali, S.; Saleh, L.; Hadi, R.; Farhoudian, S.; Nedaei, M. Transition metal oxide-based electrode materials for flexible supercapacitors : A review. *J. Alloys Compd.* **2020**, *857*, 158281. https://doi.org/10.1016/j.jallcom.2020.158281.

12. Wadekar, P.H.; Khose, R.V.; Pethsangave, D.A.; Some, S. Waste-Derived Heteroatom-Doped Activated Carbon/Manganese Dioxide Trio-Composite for Supercapacitor Applications. *Energy Technol.* **2020**, *8*, 1901402. https://doi.org/10.1002/ente.201901402.

13. Guo, W.; Yu, C.; Li, S.; Wang, Z.; Yu, J.; Huang, H.; Qiu, J. Strategies and insights towards the intrinsic capacitive properties of MnO$_2$ for supercapacitors: Challenges and perspectives. *Nano Energy* **2019**, *57*, 459–472. https://doi.org/10.1016/j.nanoen.2018.12.015.

14. Yang, D.; Ionescu, M.I. *Metal Oxide–Carbon Hybrid Materials for Application in Supercapacitors*; Elsevier Inc.: Amsterdam, The Netherlands, 2017; ISBN 9780128104644.

15. Martin-Sanchez, N.; Sanchez-Montero, M.J.; Izquierdo, C.; Salvador, F. Highlighting the role of surface groups in the gasification of carbonized raw materials of different natures with steam and supercritical water at pressures ranging from 1 to 1000 bar. *Carbon N. Y.* **2016**, *99*, 502–513. https://doi.org/10.1016/j.carbon.2015.12.072.

16. Volperts, A.; Dobele, G.; Zhurinsh, A.; Vervikishko, D.; Shkolnikov, E.; Ozolinsh, J. Wood-based activated carbons for supercapacitor electrodes with a sulfuric acid electrolyte. *Xinxing Tan Cailiao/New Carbon Mater.* **2017**, *32*, 319–326. https://doi.org/10.1016/S1872-5805(17)60125-2.

17. Veksha, A.; Sasaoka, E.; Uddin, M.A. The influence of porosity and surface oxygen groups of peat-based activated carbons on benzene adsorption from dry and humid air. *Carbon N. Y.* **2009**, *47*, 2371–2378. https://doi.org/10.1016/j.carbon.2009.04.028.

18. Xiao, N.; Wei, Y.; Li, H.; Wang, Y.; Bai, J.; Qiu, J. Boosting the sodium storage performance of coal-based carbon materials through structure modification by solvent extraction. *Carbon N. Y.* **2020**, *162*, 431–437. https://doi.org/10.1016/j.carbon.2020.02.015.

19. Li, C.; Wang, Y.; Xiao, N.; Li, H.; Ji, Y.; Guo, Z.; Liu, C.; Qiu, J. Nitrogen-doped porous carbon from coal for high efficiency CO$_2$ electrocatalytic reduction. *Carbon N. Y.* **2019**, *151*, 46–52. https://doi.org/10.1016/j.carbon.2019.05.042.

20. Li, G.Q.; Tian, F.H.; Zhang, Y.F.; Ding, J.L.; Fu, Y.L.; Wang, Y.; Zhang, G.J. Bamboo/lignite-based activated carbons produced by steam activation with and without ammonia for SO$_2$ adsorption. *Xinxing Tan Cailiao/New Carbon Mater.* **2014**, *29*, 486–492. https://doi.org/10.1016/j.carbon.2014.12.083.

21. Starck, J.; Burg, P.; Muller, S.; Bimer, J.; Furdin, G.; Fioux, P.; Vix-Guterl, C.; Begin, D.; Faure, P.; Azambre, B. The influence of demineralisation and ammoxidation on the adsorption properties of an activated carbon prepared from a Polish lignite. *Carbon N. Y.* **2006**, *44*, 2549–2557. https://doi.org/10.1016/j.carbon.2006.05.052.

22. Wei, L.; Yushin, G. Nanostructured activated carbons from natural precursors for electrical double layer capacitors. *Nano Energy* **2012**, *1*, 552–565. https://doi.org/10.1016/j.nanoen.2012.05.002.

23. Tabac, S.; Eisenberg, D. Pyrolyze this paper: Can biomass become a source for precise carbon electrodes? *Curr. Opin. Electrochem.* **2021**, *25*, 100638.

24. Vallero, D. Air Pollutant Emissions. In *Fundamentals of Air Pollution*; Elsevier: Amsterdam, The Netherlands, 2014.; pp. 787–827.

25. Tan, M.H.; Zheng, J.T.; Li, P.; Noritatsu, T.; Wu, M.B. Preparation and modification of high performance porous carbons from petroleum coke for use as supercapacitor electrodes. *Xinxing Tan Cailiao/New Carbon Mater.* **2016**, *31*, 343–351. https://doi.org/10.1016/S1872-5805(16)60018-5.

26. Lu, Q.; Xu, Y.Y.; Mu, S.J.; Li, W.C. The effect of nitrogen and/or boron doping on the electrochemical performance of non-caking coal-derived activated carbons for use as supercapacitor electrodes. *Xinxing Tan Cailiao/New Carbon Mater.* **2017**, *32*, 442–450. https://doi.org/10.1016/S1872-5805(17)60133-1.

27. Wei, F.; Zhang, H.F.; He, X.J.; Ma, H.; Dong, S.A.; Xie, X.Y. Synthesis of porous carbons from coal tar pitch for high-performance supercapacitors. *Xinxing Tan Cailiao/New Carbon Mater.* **2019**, *34*, 132–139. https://doi.org/10.1016/S1872-5805(19)60006-5.

28. Tang, W.; Zhang, Y.; Zhong, Y.; Shen, T.; Wang, X.; Xia, X.; Tu, J. Natural biomass-derived carbons for electrochemical energy storage. *Mater. Res. Bull.* **2017**, *88*, 234–241. https://doi.org/10.1016/j.materresbull.2016.12.025.

29. Dubey, P.; Shrivastav, V.; Maheshwari, P.H.; Sundriyal, S. Recent advances in biomass derived activated carbon electrodes for hybrid electrochemical capacitor applications: Challenges and opportunities. *Carbon N. Y.* **2020**, *170*, 1–29. https://doi.org/10.1016/j.carbon.2020.07.056.

30. Liang, Q.; Liu, Y.; Chen, M.; Ma, L.; Yang, B.; Li, L.; Liu, Q. Optimized preparation of activated carbon from coconut shell and municipal sludge. *Mater. Chem. Phys.* **2020**, *241*, 122327. https://doi.org/10.1016/j.matchemphys.2019.122327.

31. Martínez-Casillas, D.C.; Mascorro-Gutiérrez, I.; Arreola-Ramos, C.E.; Villafán-Vidales, H.I.; Arancibia-Bulnes, C.A.; Ramos-Sánchez, V.H.; Cuentas-Gallegos, A.K. A sustainable approach to produce activated carbons from pecan nutshell waste for environmentally friendly supercapacitors. *Carbon N. Y.* **2019**, *148*, 403–412. https://doi.org/10.1016/j.carbon.2019.04.017.

32. Jiang, L.; Yan, J.; Hao, L.; Xue, R.; Sun, G.; Yi, B. High rate performance activated carbons prepared from ginkgo shells for electrochemical supercapacitors. *Carbon N. Y.* **2013**, *56*, 146–154. https://doi.org/10.1016/j.carbon.2012.12.085.

33. Musyoka, N.M.; Mutuma, B.K.; Manyala, N. Onion-derived activated carbons with enhanced surface area for improved hydrogen storage and electrochemical energy application. *RSC Adv.* **2020**, *10*, 26928–26936. https://doi.org/10.1039/d0ra04556j.

34. Li, J.; Luo, F.; Lin, T.; Yang, J.; Yang, S.; He, D.; Xiao, D.; Liu, W. Pomelo peel-based N, O-codoped hierarchical porous carbon material for supercapacitor application. *Chem. Phys. Lett.* **2020**, *753*, 137597. https://doi.org/10.1016/j.cplett.2020.137597.

35. Ji, T.; Han, K.; Teng, Z.; Li, J.; Wang, M.; Zhang, J.; Cao, Y.; Qi, J. Synthesis of Activated Carbon Derived from Garlic Peel and Its Electrochemical Properties. *Int. J. Electrochem. Sci.* **2021**, *16*, 150653. https://doi.org/10.20964/2021.01.61.

36. Ranaweera, C.K.; Kahol, P.K.; Ghimire, M.; Mishra, S.R.; Gupta, R.K. Orange-Peel-Derived Carbon: Designing Sustainable and High-Performance Supercapacitor Electrodes. *J. Carbon Res. Artic.* **2017**, *3*, 25. https://doi.org/10.3390/c3030025.

37. Gao, Y.; Yue, Q.; Gao, B. High surface area and oxygen-enriched activated carbon synthesized from animal cellulose and evaluated in electric double-layer capacitors. *RSC Adv.* **2015**, *5*, 31375–31383. https://doi.org/10.1039/c4ra16965d.

38. Niu, L.; Shen, C.; Yan, L.; Zhang, J.; Lin, Y.; Gong, Y.; Li, C.; Sun, C.Q.; Xu, S. Waste bones derived nitrogen–doped carbon with high micropore ratio towards supercapacitor applications. *J. Colloid Interface Sci.* **2019**, *547*, 92–101. https://doi.org/10.1016/j.jcis.2019.03.097.

39. Sirengo, K.; Jande, Y.A.C.; Kibona, T.E.; Hilonga, A.; Muiva, C.; King'ondu, C.K. Fish bladder-based activated carbon/Co_3O_4/TiO_2 composite electrodes for supercapacitors. *Mater. Chem. Phys.* **2019**, *232*, 49–56. https://doi.org/10.1016/j.matchemphys.2019.04.059.

40. Elanthamilan, E.; Sriram, B.; Rajkumar, S.; Dhaneshwaran, C.; Nagaraj, N.; Princy Merlin, J.; Vijayan, A.; Wang, S.F. Couroupita guianansis dead flower derived porous activated carbon as efficient supercapacitor electrode material. *Mater. Res. Bull.* **2019**, *112*, 390–398. https://doi.org/10.1016/j.materresbull.2018.12.028.

41. Chen, H.; Yu, F.; Wang, G.; Chen, L.; Dai, B.; Peng, S. Nitrogen and Sulfur Self-Doped Activated Carbon Directly Derived from Elm Flower for High-Performance Supercapacitors. *ACS Omega* **2018**, *3*, 4724–4732. https://doi.org/10.1021/acsomega.8b00210.

42. Zheng, L.H.; Chen, M.H.; Liang, S.X.; Lü, Q.F. Oxygen-rich hierarchical porous carbon derived from biomass waste-kapok flower for supercapacitor electrode. *Diam. Relat. Mater.* **2021**, *113*, 108267. https://doi.org/10.1016/j.diamond.2021.108267.

43. Sun, W.; Lipka, S.M.; Swartz, C.; Williams, D.; Yang, F. Hemp-derived activated carbons for supercapacitors. *Carbon N. Y.* **2016**, *103*, 181–192. https://doi.org/10.1016/j.carbon.2016.02.090.

44. Roy, C.K.; Shah, S.S.; Reaz, A.H.; Sultana, S.; Chowdhury, A.N.; Firoz, S.H.; Zahir, M.H.; Ahmed Qasem, M.A.; Aziz, M.A. Preparation of Hierarchical Porous Activated Carbon from Banana Leaves for High-performance Supercapacitor: Effect of Type of Electrolytes on Performance. *Chem.—Asian J.* **2020**, *16*, 296–308. https://doi.org/10.1002/asia.202001342.

45. Boyjoo, Y.; Cheng, Y.; Zhong, H.; Tian, H.; Pan, J.; Pareek, V.K.; Jiang, S.P.; Lamonier, J.F.; Jaroniec, M.; Liu, J. From waste Coca Cola® to activated carbons with impressive capabilities for CO_2 adsorption and supercapacitors. *Carbon N. Y.* **2017**, *116*, 490–499. https://doi.org/10.1016/j.carbon.2017.02.030.

46. Boota, M.; Paranthaman, M.P.; Naskar, A.K.; Li, Y.; Akato, K.; Gogotsi, Y. Waste tire derived carbon-polymer composite paper as pseudocapacitive electrode with long cycle life. *ChemSusChem* **2015**, *8*, 3576–3581. https://doi.org/10.1002/cssc.201500866.

47. Chen, H.; Guo, Y.; Wang, F.; Wang, G.; Qi, P.; Guo, X.; Dai, B.; Yu, F. An activated carbon derived from tobacco waste for use as a supercapacitor electrode material. *Carbon N. Y.* **2018**, *130*, 848. https://doi.org/10.1016/j.carbon.2017.12.093.

48. Utetiwabo, W.; Yang, L.; Tufail, M.K.; Zhou, L.; Chen, R.; Lian, Y.; Yang, W. Electrode materials derived from plastic wastes and other industrial wastes for supercapacitors. *Chin. Chem. Lett.* **2020**, *31*, 1474–1489. https://doi.org/10.1016/j.cclet.2020.01.003.

49. Hu, X.; Lin, Z. Transforming waste polypropylene face masks into S-doped porous carbon as the cathode electrode for supercapacitors. *Ionics* **2021**, *27*, 2169–2179. https://doi.org/10.1007/s11581-021-03949-7.

50. Wang, J.; Zhang, X.; Li, Z.; Ma, Y.; Ma, L. Recent progress of biomass-derived carbon materials for supercapacitors. *J. Power Sources* **2020**, *451*, 227794. https://doi.org/10.1016/j.jpowsour.2020.227794.

51. Agbor, V.B.; Cicek, N.; Sparling, R.; Berlin, A.; Levin, D.B. Biomass pretreatment: Fundamentals toward application. *Biotechnol. Adv.* **2011**, *29*, 675–685. https://doi.org/10.1016/j.biotechadv.2011.05.005.

52. Sarkar, S.; Arya, A.; Gaur, U.K.; Gaur, A. Investigations on porous carbon derived from sugarcane bagasse as an electrode material for supercapacitors. *Biomass Bioenergy* **2020**, *142*, 105730. https://doi.org/10.1016/j.biombioe.2020.105730.

53. Ma, F.; Ding, S.; Ren, H.; Liu, Y. Sakura-based activated carbon preparation and its performance in supercapacitor applications. *RSC Adv.* **2019**, *9*, 2474–2483. https://doi.org/10.1039/c8ra09685f.

54. Kusuma, H.D.; Rochmadi; Prasetyo, I.; Ariyanto, T. Mesoporous manganese oxide/lignin-derived carbon for high performance of supercapacitor electrodes. *Molecules* **2021**, *26*, 7104. https://doi.org/10.3390/molecules26237104.

55. Wei, L.; Nitta, N.; Yushin, G. Lithographically patterned thin activated carbon films as a new technology platform for on-chip devices. *ACS Nano* **2013**, *7*, 6498–6506. https://doi.org/10.1021/nn4028129.

56. Joanna Conder, K.F.; Ghimbeu, C.M. Supercapacitors (electrochemical capacitors). In *Char and Carbon Materials Derived from Biomass Production, Characterization and Applications*; Mejdi Jeguirim, L.L., Ed.; Elsevier Inc.: Mulhouse, France, 2019; pp. 383–427, ISBN 9780128148938.

57. Xie, L.; Jin, Z.; Dai, Z.; Chang, Y.; Jiang, X.; Wang, H. Porous carbons synthesized by templating approach from fluid precursors and their applications in environment and energy storage: A review. *Carbon N. Y.* **2020**, *170*, 100–118. https://doi.org/10.1016/j.carbon.2020.07.034.

58. Gao, Y.; Yue, Q.; Gao, B.; Li, A. Insight into activated carbon from different kinds of chemical activating agents: A review. *Sci. Total Environ.* **2020**, *746*, 141094. https://doi.org/10.1016/j.scitotenv.2020.141094.

59. Abioye, A.M.; Ani, F.N. Recent development in the production of activated carbon electrodes from agricultural waste biomass for supercapacitors: A review. *Renew. Sustain. Energy Rev.* **2015**, *52*, 1282–1293. https://doi.org/10.1016/j.rser.2015.07.129.

60. Rodrfguez-reinoso, F.; Sepveda-escribano, A.; Inorgdnica, D.D.Q.; Alicante, U. De Chapter 9 Porous Carbons in Adsorption and Catalysis. In *Handbook of Surfaces and Interfaces of Materials*; Nalwa, H.S., Ed.; Academic Press: San Diego, CA, USA, 2001; Volume 5, pp. 309–355.

61. Ayinla, R.T.; Dennis, J.O.; Zaid, H.M.; Sanusi, Y.K.; Usman, F.; Adebayo, L.L. A review of technical advances of recent palm bio-waste conversion to activated carbon for energy storage. *J. Clean. Prod.* **2019**, *229*, 1427–1442. https://doi.org/10.1016/j.jclepro.2019.04.116.

62. Marsh, H.; Rodríguez-Reinoso, F. *Activation Processes (Thermal or Physical)*; Elsevier: Oxford, UK, 2006; Volume 2.

63. Pallarés, J.; González-Cencerrado, A.; Arauzo, I. Production and characterization of activated carbon from barley straw by physical activation with carbon dioxide and steam. *Biomass Bioenergy* **2018**, *115*, 64–73. https://doi.org/10.1016/j.biombioe.2018.04.015.

64. Arami-Niya, A.; Daud, W.M.A.W.; Mjalli, F.S. Comparative study of the textural characteristics of oil palm shell activated carbon produced by chemical and physical activation for methane adsorption. *Chem. Eng. Res. Des.* **2011**, *89*, 657–664. https://doi.org/10.1016/j.cherd.2010.10.003.

65. Sun, K.; Leng, C.Y.; Jiang, J.C.; Bu, Q.; Lin, G.F.; Lu, X.C.; Zhu, G.Z. Microporous activated carbons from coconut shells produced by self-activation using the pyrolysis gases produced from them, that have an excellent electric double layer performance. *Xinxing Tan Cailiao/New Carbon Mater.* **2017**, *32*, 451–459. https://doi.org/10.1016/S1872-5805(17)60134-3.

66. Kazmierczak-Razna, J.; Nowicki, P.; Wiśniewska, M.; Nosal-Wiercińska, A.; Pietrzak, R. Thermal and physicochemical proper-ties of phosphorus-containing activated carbons obtained from biomass. *J. Taiwan Inst. Chem. Eng.* **2017**, *80*, 1006–1013.

67. Şahin, Ö.; Saka, C. Preparation and characterization of activated carbon from acorn shell by physical activation with H_2O-CO_2 in two-step pretreatment. *Bioresour. Technol.* **2013**, *136*, 163–168. https://doi.org/10.1016/j.biortech.2013.02.074.

68. Heidarinejad, Z.; Dehghani, M.H.; Heidari, M.; Javedan, G.; Ali, I.; Sillanpää, M. Methods for preparation and activation of activated carbon: A review. *Environ. Chem. Lett.* **2020**, *18*, 393–415. https://doi.org/10.1007/s10311-019-00955-0.

69. Menya, E.; Olupot, P.W.; Storz, H.; Lubwama, M.; Kiros, Y. Production and performance of activated carbon from rice husks for removal of natural organic matter from water: A review. *Chem. Eng. Res. Des.* **2018**, *129*, 271–296. https://doi.org/10.1016/j.cherd.2017.11.008.

70. Wu, T.; Wang, G.; Dong, Q.; Zhan, F.; Zhang, X.; Li, S.; Qiao, H.; Qiu, J. Starch Derived Porous Carbon Nanosheets for High-performance Photovoltaic Capacitive Deionization. *Environ. Sci. Technol.* **2017**, *51*, 9244–9251. https://doi.org/10.1021/acs.est.7b01629.

71. Islam, A.; Ahmed, M.J.; Khanday, W.A.; Asif, M.; Hameed, B.H. Mesoporous activated carbon prepared from NaOH activation of rattan (*Lacosperma secundiflorum*) hydrochar for methylene blue removal. *Ecotoxicol. Environ. Saf.* **2017**, *138*, 279–285. https://doi.org/10.1016/j.ecoenv.2017.01.010.

72. Wang, L.; Sun, F.; Hao, F.; Qu, Z.; Gao, J.; Liu, M.; Wang, K. A green trace K_2CO_3 induced catalytic activation strategy for developing coal-converted activated carbon as advanced candidate for CO_2 adsorption and supercapacitors. *Chem. Eng. J.* **2019**, *383*, 123205. https://doi.org/10.1016/j.cej.2019.123205.

73. Kong, J.; Gu, R.; Yuan, J.; Liu, W.; Wu, J.; Fei, Z. Ecotoxicology and Environmental Safety Adsorption behavior of Ni (II) onto activated carbons from hide waste and high-pressure steaming hide waste. *Ecotoxicol. Environ. Saf.* **2018**, *156*, 294–300. https://doi.org/10.1016/j.ecoenv.2018.03.017.

74. Santos, S.; Cristina, R.; Bonomo, F.; Costa, R.; Fontan, I. Adsorption of the textile dye Dianix® royal blue CC onto carbons obtained from yellow mombin fruit stones and activated with KOH and H₃PO₄: Kinetics, adsorption equilibrium and thermodynamic studies. *Powder Technol.* **2018**, *339*, 334–343. https://doi.org/10.1016/j.powtec.2018.08.017.

75. Cao, L.; Yu, I.K.M.; Tsang, D.C.W.; Zhang, S.; Ok, Y.S.; Kwon, E.E.; Song, H.; Poon, C.S. Phosphoric acid-activated wood biochar for catalytic conversion of starch-rich food waste into glucose and 5-hydroxymethylfurfural. *Bioresour. Technol.* **2018**, *267*, 242–248. https://doi.org/10.1016/j.biortech.2018.07.048.

76. Legrouri, K.; Khouya, E.; Ezzine, M.; Hannache, H.; Denoyel, R.; Pallier, R.; Naslain, R. Production of activated carbon from a new precursor molasses by activation with sulphuric acid. *J. Hazard. Mater.* **2005**, *118*, 259–263. https://doi.org/10.1016/j.jhazmat.2004.11.004.

77. Wang, J.; Liu, H.; Yang, S.; Zhang, J.; Zhang, C.; Wu, H. Physicochemical characteristics and sorption capacities of heavy metal ions of activated carbons derived by activation with different alkyl phosphate triesters. *Appl. Surf. Sci.* **2014**, *316*, 443–450. https://doi.org/10.1016/j.apsusc.2014.07.206.

78. Sayğili, H.; Güzel, F. High surface area mesoporous activated carbon from tomato processing solid waste by zinc chloride activation: Process optimization, characterization and dyes adsorption. *J. Clean. Prod.* **2016**, *113*, 995–1004. https://doi.org/10.1016/j.jclepro.2015.12.055.

79. Wang, C.; Wu, D.; Wang, H.; Gao, Z.; Xu, F.; Jiang, K. A green and scalable route to yield porous carbon sheets from biomass for supercapacitors with high capacity. *J. Mater. Chem. A* **2018**, *6*, 1244–1254. https://doi.org/10.1039/c7ta07579k.

80. Cheng, H.; Wang, F.; Bian, Y.; Ji, R.; Song, Y.; Jiang, X. Co- and self-activated synthesis of tailored multimodal porous carbons for solid-phase microextraction of chlorobenzenes and polychlorinated biphenyls. *J. Chromatogr. A* **2019**, *1585*, 1–9. https://doi.org/10.1016/j.chroma.2018.11.047.

81. Wu, X.; Ding, B.; Zhang, C.; Li, B.; Fan, Z. Self-activation of potassium gluconate derived nitrogen and sulfur dual-doping hierarchical porous carbons for asymmetric supercapacitors with high energy densities. *Carbon N. Y.* **2019**, *153*, 225–233. https://doi.org/10.1016/j.carbon.2019.07.020.

82. De Yuso, A.M.; Rubio, B.; Izquierdo, M.T.Influence of activation atmosphere used in the chemical activation of almond shell on the characteristics and adsorption performance of activated carbons. *Fuel Process. Technol.* **2014**, *119*, 74–80. https://doi.org/10.1016/j.fuproc.2013.10.024.

83. Yin, J.; Zhang, W.; Alhebshi, N.A.; Salah, N.; Alshareef, H.N. Synthesis Strategies of Porous Carbon for Supercapacitor Applications. *Small Methods* **2020**, *4*, 1900853. https://doi.org/10.1002/smtd.201900853.

84. Xu, B.; Chen, Y.; Wei, G.; Cao, G.; Zhang, H.; Yang, Y. Activated carbon with high capacitance prepared by NaOH activation for supercapacitors. *Mater. Chem. Phys.* **2010**, *124*, 504–509. https://doi.org/10.1016/j.matchemphys.2010.07.002.

85. Le Van, K.; Luong Thi, T.T. Activated carbon derived from rice husk by NaOH activation and its application in supercapacitor. *Prog. Nat. Sci. Mater. Int.* **2014**, *24*, 191–198. https://doi.org/10.1016/j.pnsc.2014.05.012.

86. Basta, A.H.; Fierro, V.; El-Saied, H.; Celzard, A. 2-Steps KOH activation of rice straw: An efficient method for preparing high-performance activated carbons. *Bioresour. Technol.* **2009**, *100*, 3941–3947. https://doi.org/10.1016/j.biortech.2009.02.028.

87. Pavlenko, V.V.; Abbas, Q.; Przygocki, P.; Kon'kova, T.; Supiyeva, Z.; Abeykoon, N.; Prikhodko, N.; Bijsenbayev, M.; Kurbatov, A.; Lesbayev, B.T.; et al. Temperature dependent characteristics of activated carbons from walnut shells for improved supercapacitor performance. *Eurasian Chem. J.* **2018**, *20*, 99–105. https://doi.org/10.18321/ectj695.

88. Karagöz, S.; Tay, T.; Ucar, S.; Erdem, M. Activated carbons from waste biomass by sulfuric acid activation and their use on methylene blue adsorption. *Bioresour. Technol.* **2008**, *99*, 6214–6222. https://doi.org/10.1016/j.biortech.2007.12.019.

89. Ahmed, M.J.; Theydan, S.K. Adsorptive removal of p-nitrophenol on microporous activated carbon by FeCl₃ activation: Equilibrium and kinetics studies. *Desalin. Water Treat.* **2015**, *55*, 522–531. https://doi.org/10.1080/19443994.2014.920731.

90. Madankar, C.S.; Bhagwat, S.S.; Meshram, P.D. Cd²⁺ removal from synthetic waters by ZnCl₂-activated carbon. *Mater. Today Proc.* **2021**, *45*, 4684–4688. https://doi.org/10.1016/j.matpr.2021.01.118.

91. Li, X.R.; Jiang, Y.H.; Wang, P.Z.; Mo, Y.; Lai, W.D.; Li, Z.J.; Yu, R.J.; Du, Y.T.; Zhang, X.R.; Chen, Y. Effect of the oxygen functional groups of activated carbon on its electrochemical performance for supercapacitors. *Xinxing Tan Cailiao/New Carbon Mater.* **2020**, *35*, 232–243. https://doi.org/10.1016/S1872-5805(20)60487-5.

92. Elmouwahidi, A.; Zapata-Benabithe, Z.; Carrasco-Marín, F.; Moreno-Castilla, C. Activated carbons from KOH-activation of argan (*Argania spinosa*) seed shells as supercapacitor electrodes. *Bioresour. Technol.* **2012**, *111*, 185–190. https://doi.org/10.1016/j.biortech.2012.02.010.

93. Rehman, A.; Park, M.; Park, S.J. Current progress on the surface chemical modification of carbonaceous materials. *Coatings* **2019**, *9*, 103. https://doi.org/10.3390/COATINGS9020103.

94. Ding, Z.; Trouillet, V.; Dsoke, S. Are Functional Groups Beneficial or Harmful on the Electrochemical Performance of Activated Carbon Electrodes? *J. Electrochem. Soc.* **2019**, *166*, A1004–A1014. https://doi.org/10.1149/2.0451906jes.

95. Tran, V.M.; Ha, A.T.; Loan, M.; Le, P. Capacitance behavior of nanostructured ε-MnO₂/C composite electrode using different carbons matrix. *Adv. Nat. Sci. Nanosci. Nanotechnol.* **2014**, *5*, 025005. https://doi.org/10.1088/2043-6262/5/2/025005.

96. Adorna, J.; Borines, M.; Dang, V.D.; Doong, R.A. Coconut shell derived activated biochar–manganese dioxide nanocomposites for high performance capacitive deionization. *Desalination* **2020**, *492*, 114602. https://doi.org/10.1016/j.desal.2020.114602.

97. Dujearic-stephane, K.; Gupta, M.; Kumar, A.; Sharma, V.; Pandit, S. The Effect of Modifications of Activated Carbon Materials on the Capacitive Performance : Surface , Microstructure, and Wettability. *J. Compos. Sci.* **2021**, *5*, 66.

98. Wang, J.G.; Kang, F.; Wei, B. Engineering of MnO_2-based nanocomposites for high-performance supercapacitors. *Prog. Mater. Sci.* **2015**, *74*, 51–124. https://doi.org/10.1016/j.pmatsci.2015.04.003.

99. Wang, Y.; Liu, H.; Wang, S.; Li, X.; Wang, X.; Jia, Y. Simultaneous removal and oxidation of arsenic from water by δ-MnO_2 modifie d activate d carbon. *J. Environ. Sci.* **2020**, *94*, 147–160. https://doi.org/10.1016/j.jes.2020.03.006.

100. Bello, A.; Fashedemi, O.O.; Barzegar, F.; Madito, M.J.; Momodu, D.Y.; Masikhwa, T.M.; Dangbegnon, J.K.; Manyala, N. Microwave synthesis : Characterization and electrochemical properties of amorphous activated carbon-MnO_2 nanocomposite electrodes. *J. Alloys Compd.* **2016**, *681*, 293–300. https://doi.org/10.1016/j.jallcom.2016.04.227.

101. Song, X.; Duan, H.; Zhang, Y.; Wang, H.; Cao, H. Facile synthesis of -MnO_2/rice husk-based-activated carbon and its electrochemical properties. *Funct. Mater. Lett.* **2017**, *10*, 9–11. https://doi.org/10.1142/S1793604717500576.

102. Liu, Y.H.; Hsi, H.C.; Li, K.C.; Hou, C.H. Electrodeposited manganese dioxide/activated carbon composite as a high-performance electrode material for capacitive deionization. *ACS Sustain. Chem. Eng.* **2016**, *4*, 4762–4770. https://doi.org/10.1021/acssuschemeng.6b00974.

103. Yang, G.; Park, S.J. MnO_2 and biomass-derived 3D porous carbon composites electrodes for high performance supercapacitor applications. *J. Alloys Compd.* **2018**, *741*, 360–367. https://doi.org/10.1016/j.jallcom.2018.01.108.

104. Huang, T.; Qiu, Z.; Wu, D.; Hu, Z. Bamboo-based activated carbon @ MnO_2 nanocomposites for flexible high-performance supercapacitor electrode materials. *Int. J. Electrochem. Sci.* **2015**, *10*, 6312–6323.

105. Mohammed, A.A.; Chen, C.; Zhu, Z. Green and high performance all-solid-state supercapacitors based on MnO_2/Faidherbia albida fruit shell derived carbon sphere electrodes. *J. Power Sources* **2019**, *417*, 1–13. https://doi.org/10.1016/j.jpowsour.2019.02.003.

106. Shen, H.; Zhang, Y.; Song, X.; Liu, Y.; Wang, H.; Duan, H.; Kong, X. Facile hydrothermal synthesis of actiniaria-shaped α-MnO_2/activated carbon and its electrochemical performances of supercapacitor. *J. Alloys Compd.* **2019**, *770*, 926–933. https://doi.org/10.1016/j.jallcom.2018.08.228.

107. Yuan, C.; Lin, H.; Lu, H.; Xing, E.; Zhang, Y.; Xie, B. Synthesis of hierarchically porous MnO_2/rice husks derived carbon composite as high-performance electrode material for supercapacitors. *Appl. Energy* **2016**, *178*, 260–268. https://doi.org/10.1016/j.apenergy.2016.06.057.

108. Kong, S.; Jin, B.; Quan, X.; Zhang, G.; Guo, X.; Zhu, Q.; Yang, F.; Cheng, K.; Wang, G.; Cao, D. MnO_2 nanosheets decorated porous active carbon derived from wheat bran for high-performance asymmetric supercapacitor. *J. Electroanal. Chem.* **2019**, *850*, 113412. https://doi.org/10.1016/j.jelechem.2019.113412.

109. Performance, E.; Li, X.; Xu, M.; Yang, Y.; Huang, Q.; Wang, X.; Ren, J.; Wang, X. MnO_2 @ Corncob Carbon Composite Electrode and All-Solid-State Supercapacitor with Improved. *Materials* **2019**, *15*, 2379.

110. Wang, Y.; Liu, H.; Sun, X.; Zhitomirsky, I. Manganese dioxide-carbon nanotube nanocomposites for electrodes of electrochemical supercapacitors. *Scr. Mater.* **2009**, *61*, 1079–1082. https://doi.org/10.1016/j.scriptamat.2009.08.040.

111. Şahin, M.E.; Blaabjerg, F.; Sangwongwanich, A. A Comprehensive Review on Supercapacitor Applications and Developments. *Energies* **2022**, *15*, 674. https://doi.org/10.3390/en15030674.

112. Li, L.; Wu, Z.; Yuan, S.; Zhang, X.B. Advances and challenges for flexible energy storage and conversion devices and systems. *Energy Environ. Sci.* **2014**, *7*, 2101–2122. https://doi.org/10.1039/c4ee00318g.

113. Muzaffar, A.; Ahamed, M.B.; Deshmukh, K.; Thirumalai, J. A review on recent advances in hybrid supercapacitors: Design, fabrication and applications. *Renew. Sustain. Energy Rev.* **2019**, *101*, 123–145. https://doi.org/10.1016/j.rser.2018.10.026.